

# MASS AND LIGHT IN THE UNIVERSE<sup>1</sup>

Gillian Wilson<sup>2,3</sup>, Nick Kaiser<sup>2</sup> and Gerard A. Luppino<sup>2</sup>

`gillian@het.brown.edu`

## ABSTRACT

We present a weak lensing and photometric study of six  $0^\circ.5 \times 0^\circ.5$  degree fields observed at the CFHT using the UH8K CCD mosaic camera. The fields were observed for a total of 2 hours each in  $I$  and  $V$ , resulting in catalogs containing  $\sim 20,000$  galaxies per passband per field. We use  $V - I$  color and  $I$  magnitude to select bright early type galaxies at redshifts  $0.1 < z < 0.9$ . We measure the gravitational shear from faint galaxies in the range  $21 < m_I < 25$  from a composite catalog and find a strong correlation with that predicted from the early types if they trace the mass with  $M/L_B \simeq 300 \pm 75 hM_\odot/L_\odot$  for a flat ( $\Omega_{m0} = 0.3, \Omega_{\lambda0} = 0.7$ ) lambda cosmology and  $M/L_B \simeq 400 \pm 100 hM_\odot/L_\odot$  for Einstein-de Sitter. We make two-dimensional reconstructions of the mass surface density. Cross-correlation of the measured mass surface density with that predicted from the early type galaxy distribution shows a strong peak at zero lag (significant at the  $5.2\sigma$  level). We azimuthally average the cross- and auto-correlation functions. We conclude that the profiles are consistent with early type galaxies tracing mass on scales of  $\geq 45''$  ( $\geq 200 h^{-1}\text{kpc}$  at  $z = 0.5$ ). We sub-divide our bright early type galaxies by redshift and obtain similar conclusions. These  $M/L_B$  ratios imply  $\Omega_{m0} \simeq 0.10 \pm 0.02$  ( $\Omega_{m0} \simeq 0.13 \pm 0.03$  for Einstein-de Sitter) of closure density.

*Subject headings:* cosmology: gravitational lensing — cosmology: dark matter — cosmology: large-scale structure of universe — cosmology: observations — galaxies: photometry — galaxies: evolution

## 1. INTRODUCTION

It is well known that a large quantity of dark matter exists in the Universe. Evidence for dark matter around luminous galaxies comes from stellar velocity dispersions and rotation curves in the outer parts of spiral galaxies (Faber & Gallagher 1979; Bosma 1981; Trimble 1987); and

---

<sup>1</sup>Based on observations with the Canada-France-Hawaii Telescope which is operated by the National Research Council of Canada, le Centre National de la Recherche Scientifique de France, and the University of Hawaii.

<sup>2</sup>Institute for Astronomy, University of Hawaii, 2680 Woodlawn Drive, Honolulu, HI 96822

<sup>3</sup>Physics Department, Brown University, 182 Hope Street, Providence, RI 02912

large velocity dispersions (Faber & Gallagher 1979; Trimble 1987) and extended X-ray halos of hot gas (Mushotzky et al. 1994; Trinchieri et al. 1994; Kim & Fabbiano 1995; Trinchieri, Fabbiano, & Kim 1997) in elliptical galaxies. On larger scales, evidence for dark matter in clusters comes from gravitational lensing (Mellier 1999, and references therein), virial analyses (Carlberg et al. 1996), or X-ray halos of hot gas (White & Fabian 1995). Evidence for dark matter in the field comes from relative motions of galaxies in the Local Group (Turner 1976; Sandage 1986; Jing, Mo, & Boerner 1998), or relative motions of faint satellites (Bahcall & Tremaine 1981; Zaritsky et al. 1997), or pairs of galaxies analyzed statistically (Turner 1976; Brown & Peebles 1987; Davis, Miller, & White 1997; Jing et al. 1998). On still larger scales of  $0.25 - 3 h^{-1}\text{Mpc}$ , evidence for dark matter comes from the cosmic virial theorem analysis (Davis & Peebles 1983) and least action method (Shaya, Peebles, & Tully 1995), and on  $10 - 30 h^{-1}\text{Mpc}$  scales, from bulk flows and redshift-space anisotropies (Strauss & Willick 1995, and references therein).

The relative contribution of the dark matter component is usually specified in terms of the mass-to-light ratio,  $M/L$ , the ratio of the total mass relative to the total light within a given scale. It is generally acknowledged that the  $M/L$  ratio increases from the bright luminous regions of galaxies to their faint halos, with possible further increase on larger scale to systems such as groups and rich clusters of galaxies. The first measurement of the  $M/L$  ratio in the Coma cluster (Zwicky 1933) obtained  $M/L \sim 300 hM_{\odot}/L_{\odot}$ . Subsequent measurements of a series of clusters have confirmed his original numbers (Carlberg et al. 1997 find a virial  $M/L = 213 \pm 59$  for galaxy clusters assuming an  $\Omega_{m0} = 0.2, \Omega_{\lambda0} = 0.0$  cosmology - see also Carlberg et al. 1996). If the Coma  $M/L$  ratio is universal, then the density parameter of the Universe would appear to be  $\Omega_{m0} \simeq 0.2$ . If one wished to reconcile cluster  $M/L$  ratios with the philosophically appealing value of  $\Omega_{m0} = 1$  one was forced to argue that the efficiency of galaxy formation must therefore be biased (enhanced) in dense environments (Kaiser 1984; Bardeen et al. 1986). As one measured  $M/L$  on larger and larger scales one might expect the  $M/L$  ratio to increase until one approached the true global value of  $\Omega_{m0} = 1$ . Motivated by such reasoning, much effort has been expended, both in simulating bias on galaxy, cluster or large-scale structure scales (Davis et al. 1985) and also in attempting to measure its presence from large-scale galaxy bulk flows (Sigad et al. 1998; Willick & Strauss 1998; Branchini et al. 2000). For a time, the idea that  $M/L$  ratios increased as a function of increasing scale seemed very plausible. A very clear summary of  $M/L$  ratio with scale from a variety of methods is given in Bahcall, Lubin, & Dorman (1995, hereafter BLD). In that paper, however, it is argued, that while  $M/L$  increases with scale to  $\simeq 200 h^{-1}\text{kpc}$ , there is little evidence that  $M/L$  ratios increase on scales beyond that. BLD argued that the total mass of large-scale systems such as groups, rich clusters and superclusters could be accounted for by the total mass of their member galaxies including their large halos and intracluster gas. They argued for a  $M/L_B \simeq 100 hM_{\odot}/L_{\odot}$  for late type galaxies and a  $M/L_B \simeq 400 hM_{\odot}/L_{\odot}$  for early type galaxies and concluded that these values implied  $\Omega_{m0} \sim 0.2 - 0.3$ .

Strong evidence from Kaiser et al. (2001c, hereafter KWLKGM) also suggested a similar picture. In that paper, “A Photometric and Weak Lensing Analysis of the  $z = 0.42$  Supercluster

ms0302+17”, it was shown on scales  $\geq 200 h^{-1}\text{kpc}$  that *early* type galaxy light traces mass with  $M/L_B \simeq 250 \pm 50 h M_\odot/L_\odot$ . This was the first time that mass had been measured out to such a large radial distance ( $\simeq 3 h^{-1}\text{Mpc}$ ) from a cluster center using such a “direct” technique as gravitational lensing. This “light-traces-mass” relationship was somewhat surprising and intriguing. It raised the question of whether the relationship (and indeed  $M/L_B$  value) was exclusively applicable to early type galaxies in rich cluster environments or was applicable to early type galaxies in all environments in the Universe.

In this paper we investigate the relationship between mass and luminosity on scales of up to  $30'$  using data collected at the CFHT with the UH8K camera. Our analysis differs from previous lensing studies in that here we focus on “blank fields” i.e. the fields chosen for study were intended to be representative views of the universe which do not contain any unusually large masses such as rich clusters. We investigate the same hypothesis as proposed in KWLKGM - namely that early type galaxy light traces mass with a constant ratio of proportionality.

The outline of the paper is as follows. In §2 we describe the data and the selection of lens and background galaxies. We also present surface mass density reconstructions from shear estimates. In §3 we compare these to predictions inferred from the luminosity of early type galaxies at various redshifts. In §4 we discuss our results. We calculate the mean mass-to-light ratio of an early type galaxy and the contribution of early types to the closure density. We investigate the dependence of these values on cosmology. We then compare our values of  $M/L_B$  and  $\Omega_{m0}$  with other studies. We also consider possible sources of uncertainty. In §5 we briefly summarize our conclusions. We assume a flat lambda ( $\Omega_{m0} = 0.3, \Omega_{\lambda0} = 0.7$ ) cosmology with  $H_0 = 100 h \text{ km sec}^{-1} \text{ Mpc}^{-1}$  throughout unless explicitly stated otherwise.

## 2. THE DATA AND GALAXY SAMPLES

### 2.1. Data Acquisition and Reduction

The data were taken at the 3.6m CFHT telescope using the  $8192 \times 8192$  pixel UH8K camera at prime focus. The field of view of this camera is  $\simeq 30'$  with pixel size  $\simeq 0''.207$ . The data (six pointings) used in the analysis were acquired as part of an ongoing project whose principle aim is to investigate the cosmic shear pattern caused by gravitational lensing from the large-scale structure of the Universe. Table 1 gives an overview of the data, describing the field name, center and seeing for each pointing. This is the third in a series of papers describing results from the large-scale structure project. Kaiser, Wilson, & Luppino (2001a, Paper I, hereafter KWL) presented estimates of cosmic shear variance on  $2' - 30'$  scales, and Wilson et al. (2001b, Paper II, hereafter WKLC) investigated galaxy halos at radii of  $20'' - 60''$  ( $50 - 200 h^{-1}\text{kpc}$ ). Here we focus on mass and light on galaxy group and cluster scales. A forthcoming paper will address galaxy clustering. Further details of the data reduction pipeline may be found in Kaiser et al. (2001b), and, as already mentioned in the Introduction, an application to the ms0302 supercluster in KWLKGM. In brief, the data were

dark subtracted, flat-fielded, registered, median averaged and corrected for galactic extinction. A full description of our catalogs will be presented in a later paper (Wilson & Kaiser 2001).

## 2.2. Lens Galaxy Sample

Our analysis differs from other approaches in that we use  $V - I$  color to select a sample of bright early type lens galaxies with reasonably well determined redshifts. As we will show later, these trace the mass and thus by focusing on the distribution of early type galaxies one can accurately forecast the distribution of mass in the Universe.

As shown in section 2.2 of WKLC, with fluxes in 2 passbands one can reliably select bright early type galaxies and assign them approximate redshifts. This is because early type galaxies are the reddest galaxies at a given redshift. Thus, if we select galaxies of some color  $c$  we will see a superposition of early types at redshift  $z_E$  such that  $c = c_E(z_E)$  and later types at their appropriate, but considerably higher, redshift. An  $L \sim L_*$  early type galaxy will appear much brighter than an  $L \sim L_*$  late type galaxy by about 3 magnitudes, so with a judicious cut in red flux it is possible to isolate a bright early type galaxy sample. At lens redshift higher than  $z \simeq 0.4$ , all galaxies with colors  $V - I > 2.4$  are early types and it is unnecessary to apply any magnitude cut to exclude late types. We do, however, exclude galaxies with  $m_I$  fainter than 23.0. Figure 2 of WKLC shows  $V - I$  color versus redshift for four galaxy types and figure 1 from the same paper shows counts predicted for all galaxy types and also the specific magnitude cut we employ at each redshift to ensure that only early types remain in our sample. Table 2 shows the number of early type lens galaxies per redshift slice ( $dz = 0.1$ ) brighter than the magnitude cut (summed over all six pointings).

Table 1. Field Centers and Seeing

Field	Pointing	RA (J2000)	DEC (J2000)	l	b	FWHM(I)	FWHM(V)
Lockman	1	10:52:43.0	57:28:48.0	149.28	53.15	0".83	0".85
	2	10:56:43.0	58:28:48.0	147.47	52.83	0".84	0".86
Groth	1	14:16:46.0	52:30:12.0	96.60	60.04	0".80	0".93
	3	14:09:00.0	51:30:00.0	97.19	61.57	0".70	0".85
1650	1	16:51:49.0	34:55:02.0	57.37	38.67	0".82	0".85
	3	16:56:00.0	35:45:00.0	58.58	37.95	0".85	0".72

### 2.3. Background (Source) Galaxy Sample

The background sample was selected to lie in a range of significance  $4 < \nu < 150$  (equivalent to limiting magnitudes of  $m_I \simeq 25$  and  $m_I \simeq 21$  for a point source). Shear estimates for each galaxy,  $\hat{\gamma}_\alpha$  (for  $\alpha = 1, 2$ ), were determined using the method described in Kaiser (2000) and KWL. Weighted second moments were calculated from

$$q_\alpha = M_{\alpha lm} \int d^2r S(r) r_l r_m f(\mathbf{r}) \quad (1)$$

where  $f$  is flux;  $r$  is projected angular separation from the galaxy center;  $S$  is a Gaussian smoothing function to prevent the integral diverging at large radii; and the two constant matrices  $M_1$  and  $M_2$  are

$$M_{1lm} \equiv \begin{bmatrix} 1 & 0 \\ 0 & -1 \end{bmatrix}, \quad M_{2lm} \equiv \begin{bmatrix} 0 & 1 \\ 1 & 0 \end{bmatrix}. \quad (2)$$

Weighted second moment shapes and magnitudes of objects were measured using varying aperture photometry. The final number of galaxies per pointing and passband is shown in Table 3.

A ‘best’ combined  $IV$  catalog was also created. This is a catalog containing galaxies which have been detected in *both*  $I$  and  $V$  images above a threshold significance (of  $4\nu$ ). This is to ensure that any given “detection” is truly a real object. Shape information, i.e. shear estimates, are retained from the higher significance passband detection and discarded from the alternate passband. The galaxies tend to be detected at higher significance in the  $I$ -band images and we find that the majority ( $\simeq 80\%$ ) of galaxies in the combined  $IV$  catalog originate from the  $I$  catalog. The final number of objects in each  $IV$  catalog is shown in Table 3. (As discussed in KWL there are some low-level systematics still present in the catalogs. However, these are likely to have very little effect on the results presented in this paper for two reasons. Firstly, in this paper we analyze the light-mass cross-correlation rather than the mass auto-correlation investigated in KWL. Thus any systematic component to the shear will not correlate with the light, and is likely to average out. Secondly, we utilize mainly the  $IV$  catalog and this contains mostly galaxies originating from the  $I$ -band which was shown in KWL to be less affected by systematics than the  $V$ -band).

From galaxy shear estimates,  $\hat{\gamma}_\alpha$ , we constructed two-dimensional mass surface density reconstructions in terms of the dimensionless quantity  $\kappa$  (where  $\kappa = \Sigma/\Sigma_{\text{crit}}$ , the physical mass per unit area in units of the critical surface density). For any given lens and source galaxy redshift the critical surface density,  $\Sigma_{\text{crit}}$ , is the mass surface density required to refocus light. In the case of a distribution of background galaxy redshifts,  $\Sigma_{\text{crit}}$  becomes an average or effective mass surface density, and is given by

$$1/\Sigma_{\text{crit}} = \frac{4\pi G}{c^2} \frac{a_0 \omega_l}{1 + z_l} \langle \beta(z_l) \rangle, \quad (3)$$

where  $\omega$  is comoving distance measured in units of the current curvature scale  $a_0 = c/(H_0 \sqrt{1 - \Omega_{m0} - \Omega_{\lambda 0}})$

Table 2. Lens Galaxy Data.

Lens Redshift	Number Lens	$\Sigma_{\text{crit}}^{-1} (\times 10^{-16} h^{-1} \text{Mpc}^2 M_{\odot}^{-1})^{\text{a}}$
$0.1 \pm 0.05$	92	1.36
$0.2 \pm 0.05$	222	2.04
$0.3 \pm 0.05$	366	2.28
$0.4 \pm 0.05$	960	2.26
$0.5 \pm 0.05$	1611	2.10
$0.6 \pm 0.05$	663	1.86
$0.7 \pm 0.05$	699	1.61
$0.8 \pm 0.05$	594	1.36
$0.9 \pm 0.05$	233	1.13

<sup>a</sup>Cosmology dependent ( $\Omega_{\text{m}0} = 0.3, \Omega_{\lambda 0} = 0.7$  assumed here).

Table 3. Galaxy Catalogs.

Field	Pointing	I	V	IV
Lockman	1	20820	20358	25963
	2	20428	17782	23835
Groth	1	27906	16391	29437
	3	19300	15876	22989
1650	1	21785	15403	24494
	3	18391	16518	22894

and the dimensionless quantity  $\langle\beta(z_l)\rangle$  is defined as

$$\langle\beta(z_l)\rangle \equiv \frac{\int_0^\infty dz_s n_s(z_s)\langle W_s(z_s)\rangle\beta(z_l, z_s)}{\int_0^\infty dz_s n_s(z_s)\langle W_s(z_s)\rangle} \quad (4)$$

where  $n_s(z)$  is the redshift distribution of the source galaxies,  $\langle W_s(z_s)\rangle$  is the mean weight for source galaxies at redshift  $z_s$ , and where, finally,

$$\beta(z_l, z_s) \equiv \max(0, \sinh(\omega_s - \omega_l)/\sinh(\omega_s)) \quad (5)$$

Physically,  $\beta(z_l, z_s)$  is the ratio of the distortion induced by a lens at redshift  $z_l$  in an object at finite distance  $\omega(z_s)$  relative to that for a fictitious source at infinite distance.

For the special case of a spatially flat cosmology,  $\omega \rightarrow 0$  and  $a_0 \rightarrow \infty$ , but such that their product remains finite. In that case  $\sinh\omega \rightarrow \omega$ , and  $\langle\beta\rangle \equiv \langle\max(0, 1 - \omega_l/\omega_s)\rangle$ . For the limiting case of  $\Omega_m = 1$ ,  $\Omega_\lambda = 0$ ,  $\omega(z) = 2(1 - 1/\sqrt{1+z})$  and, in the other extreme, for  $\Omega_m \rightarrow 0$ ,  $\Omega_\lambda \rightarrow 1$ ,  $\omega(z) = z$ .

Figures 1 to 6 show two-dimensional reconstructions of  $\kappa$  using galaxy shear estimates from the catalogs described in Table 3. The Kaiser & Squires (1993) reconstruction algorithm was used. This is a stable and fast reconstruction method which has very simply defined noise properties; essentially Gaussian white noise. As with all reconstruction methods, there is a tendency for noise to increase near the data boundaries. The upper panels show the reconstructions from catalogs made from the *I* and *V*-band observations separately. The lower left panel shows the reconstruction from the composite *IV* catalog (our preferred catalog), and the lower right panel shows the reconstruction using a randomized catalog (containing the same galaxy positions as the original *IV* catalog but with randomly shuffled shear values), indicating the expected noise fluctuations due to intrinsic random galaxy shapes. The mass reconstruction from the *IV* catalog is very similar to that from the *I* catalog as might be expected if the majority of objects originated from that catalog. The reconstructions have been smoothed with a  $45''$  Gaussian filter. The wedge shows the calibration of the grayscale and the contour separation is  $0.04 \times \Sigma/\Sigma_{\text{crit}}$ .

The first thing that one notices about the mass surface density reconstructions in Figures 1 to 6 is that mass structures are much more difficult to discern than for reconstructions of clusters. At first glance, it is often somewhat unclear as to whether any given peak (or trough) in the mass reconstruction is real, or is simply a spurious noise feature due to discrete sampling of the background wallpaper of galaxies and their intrinsic ellipticities. It would be very difficult to quantify mass distributions directly from these maps.

The eye can be deceiving, however. The *I* and *V* reconstructions are actually extremely similar with regards to the positioning of the major mass distributions. Figure 7 shows the cross-correlation of the mass reconstruction from the *V* catalog with the mass reconstruction from the *I* catalog (left panel) and with the mass reconstruction from the *I* catalog with randomized shear values (right panel) for Lockman (upper) to 1650 (lower) pointings. In each case, there is a prominent peak at

zero lag. The peak is significant at the  $\sim 6 - 8\sigma$  level, depending on the pointing. That the  $I$ - and  $V$ -band signal is similar does not prove conclusively that galaxies in the  $I$  and  $V$  catalogs have been lensed by the same foreground mass structures (after all, the  $I$  and  $V$  catalogs contain many of the same objects and might simply be subject to the *same* systematics) but it is certainly reassuring.

Figure 8 illustrates more quantitatively the difficulty of teasing true signal from the noise. This figure shows two histograms of absolute pixel value from the reconstructions of mass surface density  $\kappa$  using the shear estimates from all six  $IV$  catalogs (Figures 1 to 6). The solid histogram describes originally positive pixels and the dashed histogram describes originally negative pixels. The inset shows the contrast for extreme values. Clearly the distribution is very symmetrical. Notably, a highly positive tail is absent, indicating the absence of very overdense structures e.g. rich clusters.

In view of the difficulty of measuring mass *directly* from Figures 1 to 6, and since we have a large area containing many structures, it may be possible to better reveal the signal by cross-correlating light and mass. In the following section we cross-correlate the luminosity associated with foreground galaxies with the mass inferred from the background galaxy shear estimates.

### 3. MASS AND LIGHT

#### 3.1. Mass Surface Density Predictions from Luminosity

In this section we generate predictions of the dimensional mass surface density  $\kappa$  from  $I$ -band galaxy luminosity, assuming a constant  $M/L_B$ . The implicit assumption is that optical early type galaxy luminosity is an unbiased tracer of the mass.

For a single galaxy with observed magnitude  $m_I$ , and for any cosmology, the contribution to an image of  $\kappa$  from a galaxy at redshift  $z_l$  which falls in a pixel with solid angle  $d\Omega$  is

$$\kappa d\Omega = \frac{M}{L_B} \frac{4\pi G M_\odot a_0}{c^2 (10\text{pc})^2} (1+z_l)^3 w_l \langle \beta(z_l) \rangle 10^{0.4(M_{B_\odot} - m_I + K_{BI}(z_l))} \quad (6)$$

where  $M/L_B$  is in solar units i.e.  $hM_\odot/L_\odot$ . (obtained from  $\kappa = \frac{M/dA}{\Sigma_{\text{crit}}}$  where  $A$  is area,  $M/M_\odot = M/L \times L/L_\odot$ , and  $L/L_\odot = 10^{-0.4(M_B - M_{B_\odot})}$  where  $M_{B_\odot}$  is the absolute magnitude of the sun in the B-passband and where  $K_{BI}(z) = K_I(z) - (M_B - M_I)_0$  is the combination of the conventional  $K$ -correction and the rest frame color).

From equations 3 and 6,  $\kappa$  is a function of both lens and source galaxy redshift. The lens redshift is known fairly accurately from the  $V - I$  color, but, in order to make an accurate prediction for the dimensionless surface density  $\kappa$  it is necessary to have an accurate prediction for  $\Sigma_{\text{crit}}$  and hence to have an accurate model for the redshift distribution of the faint source galaxies.

The catalogs used here are not particularly deep, and there are nearly complete redshift samples which probe similar magnitude ranges. In WKLC the catalogs were compared to the SSA22 field

sample from Cowie’s (ongoing) galaxy survey (Cowie et al. 1994; Cowie et al. 1996; Cowie, Songaila, & Barger 1999; Wilson et al. 2001a). In both of our  $I$ - and  $V$ -band samples the weight is distributed over a range of several magnitudes, with half of the weight attributed to galaxies brighter/fainter than  $m_I \simeq 23.0$  and  $m_V \simeq 24.2$ . The very faintest galaxies lie beyond the completion limit of Cowie’s sample, but the redshift distribution in a band one magnitude wide about the median magnitude is well determined. To a first approximation, the effect of variation of mean redshift with magnitude should cancel out, so one can adopt the central band redshift distribution as appropriate for the full sample. At this magnitude the samples are approximately 80% complete, and it is thought that the galaxies for which a redshift cannot be obtained lie predominantly around  $z = 1.5 - 2.0$ .

The redshift distribution was shown to be well modeled by

$$p(z) = 0.5z^2 \exp(-z/z_0)/z_0^3 \quad (7)$$

for which the mean redshift is  $\bar{z} = 3z_0$  and the median redshift is  $z_{\text{median}} = 2.67z_0$ . This is also the analytic form used by Wittman et al. (2000) and others, and seems to adequately describe the data. To allow for incompleteness we set the parameters  $n_0, z_0$  of the model distribution to match the total number of galaxies in the Cowie sample (with and without secure redshifts) and to match the mean redshift with the unmeasurable objects assigned a redshift  $z = 1.8$ . Figure 4 of WKLC shows the redshift distribution for galaxies around  $m_I = 23.0$  along with the incompleteness corrected model, which has redshift scale parameter  $z_0 = 0.39$ . The same calculation for galaxies selected in a one magnitude wide band around  $m_V = 24.2$  yields a slightly smaller, though very similar, redshift parameter  $z_0 = 0.37$ . Thus, the  $I$  and  $V$  catalogs probe to similar depth in redshift.

In Figure 9 we plot  $1/\Sigma_{\text{crit}}$  as a function of lens redshift for three cosmologies using equation 7 as the source galaxy distribution. The dot-dashed line is flat lambda ( $\Omega_{m0} = 0.3, \Omega_{\lambda0} = 0.7$ ), the solid line is Einstein-de Sitter ( $\Omega_{m0} = 1.0, \Omega_{\lambda0} = 0.0$ ), the dashed line is open baryon ( $\Omega_{m0} = 0.05, \Omega_{\lambda0} = 0.0$ ). The values of  $1/\Sigma_{\text{crit}}$  for the flat lambda case are shown in Table 2 as a function of  $z$  for redshift intervals  $dz = 0.1$ . We return to the dependence of  $M/L$  ratio on cosmology in §4.1.

To obtain the total mass surface density along the line of sight out to  $z = 1$  we use Table 2 to calculate  $\kappa = \Sigma/\Sigma_{\text{crit}}$  for each redshift slice individually and then sum the slices together. One could directly compare  $\kappa$  predicted from the light to  $\kappa$  from galaxy shear estimates obtained in §2.3. However, to ensure that our  $\kappa$ -from-light prediction is subject to the same finite-field bias and other unknown systematics as the  $\kappa$ -from-shear reconstructions, we firstly make a shear field image prediction from the constant  $M/L_B$  prediction and then sample this at the actual positions of our faint galaxies to generate a synthetic catalog (that which would have been observed with no intrinsic random shape or measurement noise), and then generate a reconstruction from that synthetic catalog. To match the spatial resolution to that of the real reconstructions (a  $45''$  Gaussian) we generate the predicted shear with smoothing scale  $45''/\sqrt{2}$  and create the reconstruction from the synthetic catalog with the same smoothing. While correctly accounting for the finite field effect on

structures within the field, the actual shear may still feel some effect from structures outside of the field.

The upper left panel of Figures 10 to 15 shows dimensionless surface mass density  $\kappa$ -from-light generated in this manner. We assumed a  $M/L_B = 300 hM_\odot/L_\odot$ . The mean has been subtracted from each image. The wedge shows the calibration of the grayscale and the contour separation is  $0.007 \times \Sigma/\Sigma_{\text{crit}}$ .

### 3.2. Mass-Light Cross-Correlation

In this section we cross-correlate light with mass. Our aim is firstly to test the hypothesis of a constant mass-to-light ratio which is independent of scale, and also later to determine the value of  $M/L_B$ , the constant of proportionality between mass and light. That is to say we are comparing the lower left panel of Figures 1-6 with the upper left panels of Figures 10-15. We also require an estimate of uncertainties inherent in the reconstruction of  $\kappa$  from the galaxy shear estimates. To obtain this we create an ensemble of 32 reconstructions for each pointing using shear values measured from the *IV* catalog, but shuffled randomly.

The left panel of Figure 16 shows the cross-correlation of light with mass averaged over all six pointings. In computing this we padded the source images with zeros to twice the original size. The right panel of Figure 16 shows the cross-correlation of light with an average over randomized catalog reconstructions. There is a strong cross-correlation peak at zero lag for the real data, which is not present for the randomized data.

The mass-to-light ratio,  $M/L_B$ , at zero lag is calculated by minimization of

$$\chi^2 = \sum_i \frac{(y_i - M/L_B x_i)^2}{\sigma_i^2} \quad (8)$$

where the sum is over the six pointings, the light auto-correlation  $x_i = \Sigma_{\text{pix}} \kappa_l \kappa_l / N_{\text{pix}}$ , the mass-light cross-correlation  $y_i = \Sigma_{\text{pix}} \kappa_m \kappa_l / N_{\text{pix}}$ , and the uncertainty is calculated from the ensemble of 32 randomized catalogs ( $\sigma_i^2 = \Sigma (y_i^{\text{rand}})^2 / N_{\text{rand}}$ ). Minimizing  $\chi^2$  with respect to  $M/L_B$ ,

$$M/L_B = \frac{\sum_i x_i y_i / \sigma_i^2}{\sum_i x_i^2 / \sigma_i^2} \quad (9)$$

The uncertainty in  $M/L_B$  is

$$\sigma_{M/L_B} = \frac{1}{\sqrt{(\sum_i x_i^2 / \sigma_i^2)}} \quad (10)$$

The significance, estimated as the strength of the zero-lag correlation relative to the rms found

from the ensemble of randomized catalogs is  $5.2\sigma$  (Table 4). That early type galaxy luminosity and total mass show such a strong correlation is the central result of this paper. The correlation strength at zero lag implies a  $M/L_B = 237 \pm 45 hM_\odot/L_\odot$ . The error is a  $1\sigma$  statistical uncertainty only and does not include any systematic error introduced into  $1/\Sigma_{\text{crit}}$  due to lack of knowledge about the redshift distribution of the source galaxies.

### 3.3. Mass-Light Cross-Correlation Profiles

In order to determine how  $M/L$  ratio varies with scale, we examine the profile of the luminosity-mass cross-correlation and luminosity auto-correlation. Figure 17 shows the azimuthally averaged profile of the mass-luminosity cross-correlation function from (open circles with error bars) and the luminosity auto-correlation function (filled circles). The luminosity auto-correlation has been normalized to 1, and in normalizing the mass-luminosity cross-correlation function, we have adopted a  $M/L_B = 250 hM_\odot/L_\odot$ , similar to that obtained at zero-lag in section 3.2. The error bars were calculated from our ensembles of 32 noise reconstructions. It is apparent from Figure 17 that although mass and luminosity do appear to trace each other, the profile is noisy, and thus it is difficult to judge if the profiles have similar shape.

In the upper left panel of Figure 18 we show the combined azimuthally averaged profile of the mass-luminosity cross-correlation function averaged over all six pointings (open circles) and the corresponding luminosity auto-correlation function (filled circles). Again, the luminosity auto-correlation has been normalized to 1 and in normalizing the mass-luminosity cross-correlation function we have adopted a  $M/L_B = 250 hM_\odot/L_\odot$ .

We see from Figure 18 that the cross- and auto- correlation functions have very similar profiles. Thus, it appears that early type galaxies trace the mass rather faithfully. We note that the profile in Figure 18 was obtained from smoothed images. The smallest scale over which mass/luminosity is being averaged is therefore  $\simeq 45''$ . We conclude therefore that on scales  $\geq 45''$  our results are consistent with early type galaxies tracing mass.

### 3.4. Mass and Light as a Function of Redshift

In this section we investigate  $M/L$ , the constant of proportionality between mass and light, as a function of redshift. We divide our data into three slices, each of size width  $dz = 0.3$  (Table 4) and analyze each slice separately.

Figures 10 to 15 show the dimensionless surface mass density prediction  $\kappa$ -from-light generated as described in Section 3.1. The remaining three panels in each figure show  $\kappa$ -from-light summed over three redshift slices intervals centered on  $z = 0.2$ ,  $z = 0.5$ , and  $z = 0.8$  rather than the sum over all nine redshift intervals described in § 3.1. We again assume a  $M/L_B = 300 hM_\odot/L_\odot$  and

Table 4.  $M/L_B$  Values at Zero Lag.

$\Omega_{m0}$	$\Omega_{\lambda0}$	Lens Redshift	Number Lens	$\Sigma_{\text{crit}}^{-1} (\times 10^{-16} h^{-1} \text{Mpc}^2 M_{\odot}^{-1})$	$M/L_B$	$\nu$
Flat Lambda						
0.3	0.7	$0.5 \pm 0.45$	5440	1.91	$237 \pm 45$	5.2
0.3	0.7	$0.2 \pm 0.15$	680	2.08	$353 \pm 67$	5.3
0.3	0.7	$0.5 \pm 0.15$	3234	2.10	$272 \pm 75$	3.6
0.3	0.7	$0.8 \pm 0.15$	1526	1.44	$-61 \pm 143$	-0.4
Einstein-de Sitter						
1.0	0.0	$0.5 \pm 0.45$	5018	1.39	$294 \pm 60$	4.9
1.0	0.0	$0.2 \pm 0.15$	526	1.72	$385 \pm 82$	4.7
1.0	0.0	$0.5 \pm 0.15$	2966	1.54	$376 \pm 101$	3.7
1.0	0.0	$0.8 \pm 0.15$	1526	0.98	$-93 \pm 211$	-0.4

use equations 3 and 6. Luminosity is binned into equal angular-size pixels and we note that since our field of view corresponds to a different physical extent with redshift ( $2.32 h^{-1}\text{Mpc}$  at  $z = 0.1$ ;  $9.82 h^{-1}\text{Mpc}$  at  $z = 0.9$ ) the binsize is similarly a function of redshift. It is apparent from Figures 10 to 15 that most of the  $\kappa$ -from-light signal originates at low and intermediate redshift.

This effect can also be seen in Figure 19. The left panels show the cross-correlation of light with mass averaged over all six pointings as a function of redshift. The right panels show the cross-correlation of light with an average over randomized shear catalog reconstructions. The slices centered on redshifts  $z = 0.2$  and  $z = 0.5$  show a strong cross-correlation peak at zero lag. The correlation strength at zero lag implies a  $M/L_B = 353 \pm 67 hM_\odot/L_\odot$  for  $z = 0.2$  with  $5.3\sigma$  significance and  $M/L_B = 272 \pm 75 hM_\odot/L_\odot$  for  $z = 0.5$  with  $3.6\sigma$  significance (Table 4). The highest redshift slice shows no such peak, and a  $M/L_B$  consistent with zero ( $-60 \pm 143 hM_\odot/L_\odot$ ).

Figure 18 shows the azimuthally averaged profile of the mass-luminosity cross-correlation function from (open circles with error bars) and the luminosity auto-correlation function (filled circles). The redshift interval is marked on each panel. Again, the luminosity auto-correlation has been normalized to 1 but for better comparison of the profiles, in normalizing the mass-luminosity cross-correlation function here we have adopted a higher  $M/L_B = 300 hM_\odot/L_\odot$ , more similar to that obtained at zero-lag (rather than the  $M/L_B = 250 hM_\odot/L_\odot$  used for the whole sample in section 3.3). As before, uncertainties were calculated from 32 reconstructions using randomly shuffled shear values from our *IV* catalog.

There is perhaps some very slight evidence from Figure 18 that the mass-luminosity profile might be more extended than the luminosity-luminosity profile. An extended mass-luminosity profile would be expected if a) any mass associated with late type galaxies were non-negligible, and b) one takes into account the known fact that late type galaxies are clustered around early types (Davis & Geller 1976) but are more weakly clustered than early types around early types. A more realistic scenario, therefore, might include both early and late type galaxies, with a slightly lower  $M/L_B$  for early types than quoted here, and an additional much lower but non-zero  $M/L_B$  for late types (the mass associated with late types cannot be dominant compared to the early types or we would not see such a strong mass-to-early-type-luminosity correlation in Figure 16). Further data will be required to determine conclusively whether the mass-luminosity profile is actually extended and not simply a noise artifact. For now, however, we conclude, that within the uncertainties of this dataset, we find no evidence for (early type galaxy) luminosity and (total) mass segregation: it does appear that early type galaxies trace the mass very similarly at all redshifts.

We note from Figure 18 that the uncertainties increase with increasing redshift. This is easily understandable when one realizes from equation 9 that, if the pointings have similar noise properties as they do here, the mass-light correlation essentially consists of the product of  $\kappa$ -from-shear and  $\kappa$ -from-light divided by the product  $\kappa$ -from-light squared.

$$M/L_B \rightarrow \frac{\sum_{\text{pix}} \kappa_m \kappa_l}{\sum_{\text{pix}} \kappa_l \kappa_l} \quad (11)$$

Each factor of  $\kappa$ -from-light (equation 6) contains a factor of  $1/\Sigma_{\text{crit}}$  which at high redshifts becomes very small (Figure 9). Thus for higher redshift lenses, one is dividing a fixed uncertainty in the numerator (the uncertainty in  $\kappa_m$  due to intrinsic galaxy ellipticities) by one factor of the decreasing quantity  $1/\Sigma_{\text{crit}}$ , and hence the uncertainty in the quotient, the mass-to-light ratio, increases with redshift. One could reduce the uncertainty in mass-to-light ratio at larger redshift if one had deeper catalogs i.e. catalogs containing source galaxies at higher redshift. Thus, one should not interpret Figures 10 to 15, and 18 to 19 as implying that there is negligible mass at redshift  $z \geq 0.8$ , but rather, that without deeper catalogs one should not expect to be able to detect it.

The value of  $M/L_B$  ( $\simeq 300 hM_\odot/L_\odot$ ) obtained for the two lower redshift slices ( $z = 0.2$  and  $z = 0.5$ ) was higher than that obtained for the combined sample. We interpret a depressed  $M/L_B$  value for the combined sample as a dilution effect due to the inclusion of high redshift ( $z = 0.6-0.9$ ) early types whose luminosity contributes to the auto-correlation (denominator) of equation 11 but whose mass does not contribute to the numerator because of the reasons discussed in the previous paragraph.

The  $M/L_B$  value of  $\simeq 300 hM_\odot/L_\odot$  obtained from the two lower redshift slices is therefore most likely to be representative for this cosmology, and this is the value we shall adopt for the remainder of the paper.

#### 4. DISCUSSION

In the previous sections we used our CFHT data to cleanly select a sample of bright early type galaxies using  $V - I$  colors and  $I$  magnitudes, and assign reasonably precise redshifts to them. We showed that there was a strong correlation between the actual mass inferred from weak lensing analysis and the mass predicted assuming the light associated with early type galaxies traces mass with a constant mass-to-light ratio.

This is a surprising result which was first noticed for the ms0302 supercluster by KWLKGMD, as discussed in the Introduction. The caveat, in that case, of course, was that as with all examples of *cluster* measurements there was a strong possibility of bias and no guarantee that a cluster  $M/L$  ratio was representative of the Universe in general. There may have been something unusual about the way that galaxies formed in such extremely overdense environments as clusters which was not reproduced elsewhere under more “normal” conditions of formation. In this paper we have demonstrated the remarkable result that early type galaxy light traces mass with constant  $M/L$  ratio appears to be a universally applicable relationship.

#### 4.1. $M/L_B$ in an Einstein-de Sitter universe

The actual value of the constant of proportionality between mass and light is dependent upon cosmology. We performed our analysis assuming a flat lambda ( $\Omega_{m0} = 0.3, \Omega_{\lambda0} = 0.7$ ) cosmology. We also repeated the analysis for an Einstein-de Sitter ( $\Omega_{m0} = 1.0, \Omega_{\lambda0} = 0.0$ ) cosmology. The required  $M/L_B$  ratio *increases* if this cosmology is assumed. Values of  $M/L_B$  at zero lag are shown in Table 4. The dependence of  $M/L_B$  on cosmology can be understood qualitatively from the following argument. From (4) it is clear that the predicted  $\kappa$ -from-light is a function of  $1/\Sigma_{\text{crit}}$ . From Figure 9 it is clear that for an Einstein-de Sitter cosmology,  $1/\Sigma_{\text{crit}}$  is smaller than for the flat lambda case at all redshift. Thus, the predicted  $\kappa$ -from-light in this cosmology is smaller by the same scaling factor. Note that the scaling factor is not constant, but is a function of redshift, being the ratio of the height of the solid to dot-dashed line at each redshift. Hence, for this cosmology in order to match the same  $\kappa$  fluctuations obtained from the  $\kappa$ -from-shear analysis, a *higher* value of  $M/L_B$  ratio is required.

#### 4.2. Comparison with other Galaxy Groups/Cluster Studies

$M/L$  ratios have been measured on galaxy group and cluster scales by several other teams. On group scales, Hoekstra, Franx, & Kuijken (1999) recently found an average  $M/L_B = 372 \pm 122$  for galaxy groups, after making a correction for luminosity evolution. On larger scales, Mellier (1999, Table 1 and references therein) summarize all published  $M/L$  ratios obtained for clusters using gravitational lensing as of 1999. One should be cautious because the different teams used different telescopes, software packages and mass reconstruction techniques, and obtained data under varying seeing and to varying physical radii from the cluster center. Additionally, some teams choose to quote  $M/L_V$  in preference to  $M/L_B$ . Nevertheless, on scales of about 1 Mpc, the geometry of each cluster mass distribution inferred from gravitational lensing was similar to the galaxy distribution, and also the X-ray distribution when it was available. The  $M/L$  ratios obtained by different teams are fairly scattered, but have a median value of 300, with a trend to increase with radius. As clusters contain a high fraction of elliptical galaxies it is not so unexpected that  $M/L$  ratios for clusters turn out to be so similar to the value we derive in this paper.

#### 4.3. Inferred Mass Density $\Omega_{m0}$

We now calculate  $\Omega_{m0}$ , the fractional contribution of early type galaxy mass density to the critical mass density (where  $\rho_{\text{crit}} = 2.77 \times 10^{11} h^2 M_{\odot} \text{Mpc}^{-3}$ ),

$$\Omega_{m0} = \rho_E / \rho_{\text{crit}} \tag{12}$$

$$\rho_E = (M/L)_E \mathcal{L}_E = (M/L)_E \phi_{\star E} L_{\star E} \Gamma(\alpha_E + 2) \quad (13)$$

where  $\mathcal{L}_E$  is the measured  $B$ -band early type luminosity density of the universe for *early* type galaxies. With  $\phi_{\star E}$  of  $9 \times 10^{-3} (h^{-1} \text{Mpc})^{-3}$ ,  $L_{\star E}$  of  $-19.61$ , and  $\alpha_E$  of  $-0.74$  (from Folkes et al. 1999), we obtain  $\mathcal{L}_E = 8.83 \times 10^7 h L_{\odot} \text{Mpc}^{-3}$ .

Using our  $M/L_B$  estimates for early types, and assuming a  $M/L$  ratio of  $300 h M_{\odot}/L_{\odot}$  (400 for Einstein-de Sitter) and an uncertainty of  $\pm 25\%$  (the uncertainty in our  $M/L_B$  value is a much greater contribution to the error budget than the uncertainty from Folkes et al.), we obtain  $\Omega_{m0} \simeq 0.10 \pm 0.02$  of closure density ( $\Omega_{m0} \simeq 0.13 \pm 0.03$  for Einstein-de Sitter).

The global density parameter we obtain appears low compared to other estimates (Carlberg et al. 1997; Mellier 1999). This is not because our early type  $M/L_B$  value is low but because we do not assign the same  $M/L_B$  to late types as to early types. In the scenario we propose, late types are assumed to have very similar luminosities as early types (e.g. Folkes et al. (1999) find  $B_{\star}$  for late types to be very similar to  $B_{\star}$  for early types). The difference is that late types have much less mass associated with them and hence their  $M/L_B$  ratio is much lower. The analysis in this paper assumes that they have negligible  $M/L_B$  compared to early types.

Interestingly, we note that the current best limit on the baryon fraction determined from Big Bang nucleosynthesis measurements, assuming  $H_0 = 65 \text{ km sec}^{-1} \text{ Mpc}^{-1}$ , is  $\Omega_B = 0.045 \pm 0.0028$  ( $\Omega_B h^2 = 0.019 \pm 0.0012$  from Burles et al. 2000). From (4) and Figure 9 one would expect the  $M/L_B$  ratio for an open baryon ( $\Omega_{m0} = 0.05$ ) universe  $\simeq 350 h M_{\odot}/L_{\odot} \pm 25\%$ , intermediate between the flat lambda and Einstein-de Sitter values. The lower limit to the mass fraction is thus rather close to the baryon-only fraction suggesting that baryons might be the sole source of mass in the universe. A flat lambda cosmology with  $\Omega_{m0} = 0.05$  in baryons would require an  $M/L_B$  ratio *smaller* than that found for our fiducial  $\Omega_{m0} = 0.3$  case which would in turn *decrease* the estimates of  $\Omega_{m0} \sim 0.10 \pm 0.02$  found above. We also note in passing that preliminary analyses of recent CMB measurements (Jaffe 2000) prefer a higher value for  $\Omega_B = 0.076 \pm 0.012$  ( $\Omega_B h^2 = 0.032 \pm 0.005$ ) than that derived by Burles et al.. Of course, the upper limit we obtain for the mass fraction is triple the baryon-only fraction and would require sizeable quantities of exotic matter. Additionally, other measurements, in particular supernovae constraints, suggest the Universe may contain quantities of exotic matter. Note also that all mass reconstructions from weak lensing analyses are blind to any uniform density component so in actuality, our  $M/L_B$  ratios should be considered to be lower limits.

#### 4.4. Possible Uncertainties

As a consistency check, we repeated the mass-luminosity correlation analysis in § 3 but for  $I$  and  $V$  band catalogs separately. We obtained similar values of significance and  $M/L_B$  (within our 25% uncertainties) as a function of redshift as had been obtained for the best composite catalog.

The value of  $M/L_B$  we infer is strongly dependent on both cosmology and source redshift distribution. Although we believe the effect of any uncertainty in the redshift distribution of the source galaxies is largely dwarfed by intrinsic galaxy shape and measurement errors we note that if the redshift distribution were in error and source galaxies were in fact at higher (lower) redshift than our estimate, the inferred  $M/L_B$  ratio would decrease (increase).

Additionally, if there were some evolution in  $L_*$  such that galaxies were brighter by a few tenths of a magnitude between  $z = 0.5$  and the present, this would force an upward revision to the  $M/L_B$  ratio inferred for the  $z = 0.5 \pm 0.15$  sample. That the  $z = 0.2 \pm 0.15$  and  $z = 0.5 \pm 0.15$   $M/L_B$  values are so similar (Table 4) argues against strong luminosity evolution in the early types between redshift 0.5 and the present.

In the analysis performed in this paper we were forced by the availability of only two passbands to select early type galaxies within 1 – 2 magnitudes of  $L_*$ . Presumably,  $M/L_B$  might not be constant with decreasing luminosity. However, the  $M/L_B$  ratio cannot increase dramatically at the faint end of the luminosity function i.e. faint galaxies cannot be very massive relative to their luminosity or the correlation between mass and bright early type light seen in Figure 16 would not be so convincing. Also, there is of course, some mass associated with late type galaxies. Any mass associated with late type galaxies will contribute to the noise in Figures 16 and 19. However, as mentioned in §3.4 it cannot be dominant compared to the early types or again, we would not see such a strong mass-to-early-type-luminosity correlation.

Note that the values of  $M/L_B$  derived in this paper are entirely consistent with  $M/L_B$  ratios for galaxy halos derived in WKLC from a galaxy-galaxy lensing analysis. In that paper, we found a typical mass-to-light ratio of  $M/L_B \simeq 121 \pm 28h(r/100 h^{-1}\text{kpc})$  (for  $L_*$  galaxies). In this paper, we found that halos extend to  $\simeq 2'$  at  $z \sim 0.2$  (Figure 18) which corresponds to  $r \sim 280 h^{-1}\text{kpc}$ . Within that radius we therefore predict a  $M/L_B$  of  $2.8 \times 121 \pm 28 hM_\odot/L_\odot = 340 \pm 80 hM_\odot/L_\odot$  from that paper (assuming a flat lambda ( $\Omega_{m0} = 0.3, \Omega_{\lambda0} = 0.7$ ) cosmology) which compares well with the  $M/L_B$  of  $300 \pm 75 hM_\odot/L_\odot$  derived from this paper.

We note, that in WKLC we adopted a different relationship between galaxy mass and light. On small scales ( $\lesssim 10 h^{-1}\text{kpc}$ ) it has been shown empirically that mass is approximately proportional to the square root of luminosity of early type galaxies i.e.  $M \propto \sqrt{L}$  (Faber & Jackson 1976; Fukugita & Turner 1991). In this paper we are probing scales larger than individual galaxy halos, and it seems more reasonable to assume  $M \propto L$  on these scales. Incidentally, the  $M \propto \sqrt{L}$  relationship on small scales also justifies our choice of smoothing scale ( $45'' \sim 200 h^{-1}\text{kpc}$  at  $z = 0.5$ ). A smoothing scale of a few hundred  $h^{-1}\text{kpc}$  ensures we are investigating scales “one step up” from individual galaxy halos where  $M/L$  biases on very small scales would tend to average out.

Based on the dataset described in this paper, it would be premature to claim definitively that (early type galaxy) luminosity traces mass with a *constant* mass-to-light ratio. The luminosity-luminosity and mass-luminosity profiles do appear remarkably similar. However, the uncertainties are sizeable ( $\simeq 25\%$ ). We conclude that there is no evidence for (early type galaxy) luminosity

and mass segregation on galaxy group and cluster scales but that larger quantities of data will be required to determine empirically the mass-to-luminosity dependence to greater precision. That mass should be directly proportional to luminosity is a very appealing relationship but nature may have conspired otherwise, and there may well still be scope for some amount of biased galaxy formation.

## 5. CONCLUSIONS

Using  $V - I$  color and  $I$  magnitude we cleanly selected bright early type galaxies. We measured the gravitational shear from faint galaxies and found a strong correlation with that predicted from the early types if they trace the mass with  $M/L_B \simeq 300 \pm 75 hM_\odot/L_\odot$  for a flat ( $\Omega_{m0} = 0.3, \Omega_{\lambda0} = 0.7$ ) lambda cosmology and  $M/L_B \simeq 400 \pm 100 hM_\odot/L_\odot$  for Einstein-de Sitter. We made two-dimensional reconstructions of the mass surface density. Cross-correlation of the measured mass surface density with that predicted from the early type galaxy distribution showed a strong peak at zero lag. We azimuthally averaged the cross- and auto-correlation functions. We concluded that the profiles were consistent with early type galaxies tracing mass on scales of  $\geq 45''$  (the smoothing scale). We subdivided our bright early type galaxies by redshift and obtained similar conclusions. These  $M/L_B$  ratios imply  $\Omega_{m0} \simeq 0.10 \pm 0.02$  ( $\Omega_{m0} \simeq 0.13 \pm 0.03$  for Einstein-de Sitter) of closure density.

In summary, we found that the majority of mass in the universe is associated with early type galaxies. On scales of  $\geq 200 h^{-1}\text{kpc}$  it appears that their light traces the underlying mass distribution with a constant  $M/L_B = 300 - 400 \pm 100 hM_\odot/L_\odot$ , depending on cosmology. As with several other recent results our data argues against an  $\Omega_{m0} = 1$  universe.

In the future it will be possible to measure  $M/L_B$  ratios more precisely. The total areal coverage in this paper was  $1.5 \text{ deg}^2$ . Future planned surveys such as the Hawaii Lensing Survey, the Deep Lens Survey, or the Megacam/Terapix consortium will cover much larger area and hence reduce uncertainties in  $M/L_B$ . Additionally, more precise constraints on cosmology ( $\Omega_{m0}$  and  $\Omega_{\lambda0}$ ) should soon be available from cosmic microwave background measurements, supernovae and the deep lensing surveys themselves. The color-redshift degeneracy could be broken by an increased number of passbands to provide photometric redshifts. The greater range of absolute luminosity then available (limited here to  $L \sim L_* \pm 1 - 2$ ) would allow mass-to-luminosity dependence (assumed in this work to be  $M \propto L$ ) to be determined more precisely, both as a function of luminosity and as a function of distance from galaxy center. Finally, the availability of  $> 2$ -passband data would also allow photometric redshifts to be determined for late type galaxies and a similar investigation to be undertaken into their  $M/L$  ratios.

We thank Douglas Burke and Len Cowie for many useful discussions. We also thank Marc Davis, the referee, for his constructive comments. GW gratefully acknowledges financial support

from the estate of Beatrice Watson Parrent and from Mr. & Mrs. Frank W. Hustace, Jr. whilst Parrent Fellow at UH. This work was supported by NSF grant AST99-70805.

## REFERENCES

- Bahcall, J. N. & Tremaine, S. 1981, *ApJ*, 244, 805
- Bahcall, N. A., Lubin, L. M., & Dorman, V. 1995, *ApJ*, 447, L81
- Bardeen, J. M., Bond, J. R., Kaiser, N., & Szalay, A. S. 1986, *ApJ*, 304, 15
- Bosma, A. 1981, *AJ*, 86, 1825
- Branchini, E., Zehavi, I., Plionis, M., & Dekel, A. 2000, *MNRAS*, 313, 491
- Brown, M. E. & Peebles, P. J. E. 1987, *ApJ*, 317, 588
- Burles, S., Nollett, K. M., Truran, J. M., & Turner, M. S. 2000, preprint (astro-ph/9901157)
- Carlberg, R. G., Yee, H. K. C., & Ellingson, E. 1997, *ApJ*, 478, 462
- Carlberg, R. G., Yee, H. K. C., Ellingson, E., Abraham, R., Gravel, P., Morris, S., & Pritchett, C. J. 1996, *ApJ*, 462, 32
- Cowie, L. L., Gardner, J. P., Hu, E. M., Songaila, A., Hodapp, K. W., & Wainscoat, R. J. 1994, *ApJ*, 434, 114
- Cowie, L. L., Songaila, A., & Barger, A. J. 1999, *AJ*, 118, 603 (CSB)
- Cowie, L. L., Songaila, A., Hu, E. M., & Cohen, J. G. 1996, *AJ*, 112, 839
- Davis, M., Efstathiou, G., Frenk, C. S., & White, S. D. M. 1985, *ApJ*, 292, 371
- Davis, M. & Geller, M. J. 1976, *ApJ*, 208, 13
- Davis, M., Miller, A., & White, S. D. M. 1997, *ApJ*, 490, 63
- Davis, M. & Peebles, P. J. E. 1983, *ApJ*, 267, 465
- Faber, S. M. & Gallagher, J. S. 1979, *ARA&A*, 17, 135
- Faber, S. M. & Jackson, R. E. 1976, *ApJ*, 204, 668
- Folkes, S., Ronen, S., Price, I., Lahav, O., Colless, M., Maddox, S., Deeley, K., Glazebrook, K., et al., 1999, *MNRAS*, 308, 459
- Fukugita, M. & Turner, E. L. 1991, *MNRAS*, 253, 99

- Hoekstra, H., Franx, M., & Kuijken, K. 1999, preprint, astrophys/9911106
- Jaffe, A. 2000, preprint (astro-ph/0007333)
- Jing, Y. P., Mo, H. J., & Boerner, G. 1998, ApJ, 494, 1
- Kaiser, N. 1984, ApJ, 284, L9
- . 2000, ApJ, 537, 555
- Kaiser, N. & Squires, G. 1993, ApJ, 404, 441
- Kaiser, N., Wilson, G., & Luppino, G. 2001a, paper I, cosmic shear paper, preprint (astro-ph/0003338), KWL
- Kaiser, N., Wilson, G., Luppino, G., & Dahle, H. 2001b, preprint (astro-ph/9907229), KWLD
- Kaiser, N., Wilson, G., Luppino, G., Kofman, L., Gioia, I., Metzger, M., & Dahle, H. 2001c, preprint (astro-ph/9809268), KWLKGMD
- Kim, D. & Fabbiano, G. 1995, ApJ, 441, 182
- Mellier, Y. 1999, ARA&A, 37, 127
- Mushotzky, R. F., Loewenstein, M., Awaki, H., Makishima, K., Matsushita, K., & Matsumoto, H. 1994, ApJ, 436, L79
- Sandage, A. 1986, ApJ, 307, 1
- Shaya, E. J., Peebles, P. J. E., & Tully, R. B. 1995, ApJ, 454, 15
- Sigad, Y., Eldar, A., Dekel, A., Strauss, M. A., & Yahil, A. 1998, ApJ, 495, 516
- Strauss, M. A. & Willick, J. A. 1995, Phys. Rep., 261, 271
- Trimble, V. 1987, ARA&A, 25, 425
- Trinchieri, G., Fabbiano, G., & Kim, D. 1997, A&A, 318, 361
- Trinchieri, G., Kim, D., Fabbiano, G., & Canizares, C. R. C. 1994, ApJ, 428, 555
- Turner, E. L. 1976, ApJ, 208, 304
- White, D. A. & Fabian, A. C. 1995, MNRAS, 273, 72
- Willick, J. A. & Strauss, M. A. 1998, ApJ, 507, 64
- Wilson, G., Cowie, L. L., Barger, A. J., & Burke, D. J. 2001a, star formation rates in the Hawaii Survey Fields, in prep.

Wilson, G. & Kaiser, N. 2001, paper V, UH8K catalog paper, in prep

Wilson, G., Kaiser, N., Luppino, G., & Cowie, L. L. 2001b, paper II, galaxy-galaxy paper, submitted to ApJ, preprint (astro-ph/0008504), WKLC

Wittman, D. M., Tyson, J. A., Kirkman, D., Dell’Antonio, I., & Bernstein, G. 2000, Nature, 405, 143

Zaritsky, D., Smith, R., Frenk, C., & White, S. D. M. 1997, ApJ, 478, 39

Zwicky, F. 1933, Helv. Phys. Acta. 6, 110

Fig. 1.— Upper panels show reconstructions of mass surface density  $\kappa$  ( $= \Sigma/\Sigma_{\text{crit}}$ ) made from the  $I$ - and  $V$ -band catalogs separately for Lockman field (pointing 1). The lower left panel shows the reconstruction from the composite  $IV$  catalog, and the lower right panel shows the reconstruction from the same catalog with randomized ellipticities, indicating the expected noise fluctuations due to intrinsic random galaxy shapes. The reconstructions have been smoothed with a  $45''$  Gaussian filter. The wedge shows the calibration of the grayscale and the contour separation is  $0.04 \times \Sigma/\Sigma_{\text{crit}}$ .

Fig. 2.— Same as for Figure 1 but for Lockman field (pointing 2).

Fig. 3.— Same as for Figure 1 but for Groth field (pointing 1).

Fig. 4.— Same as for Figure 1 but for Groth field (pointing 3).

Fig. 5.— Same as for Figure 1 but for 1650 field (pointing 1).

Fig. 6.— Same as for Figure 1 but for 1650 field (pointing 3).

Fig. 7.— Cross-correlation of mass reconstruction from the  $V$  catalog with mass reconstruction from the  $I$  catalog (left panel) and with mass reconstruction from the randomized  $I$  catalog (right panel) for Lockman (upper) to 1650 (lower) fields.

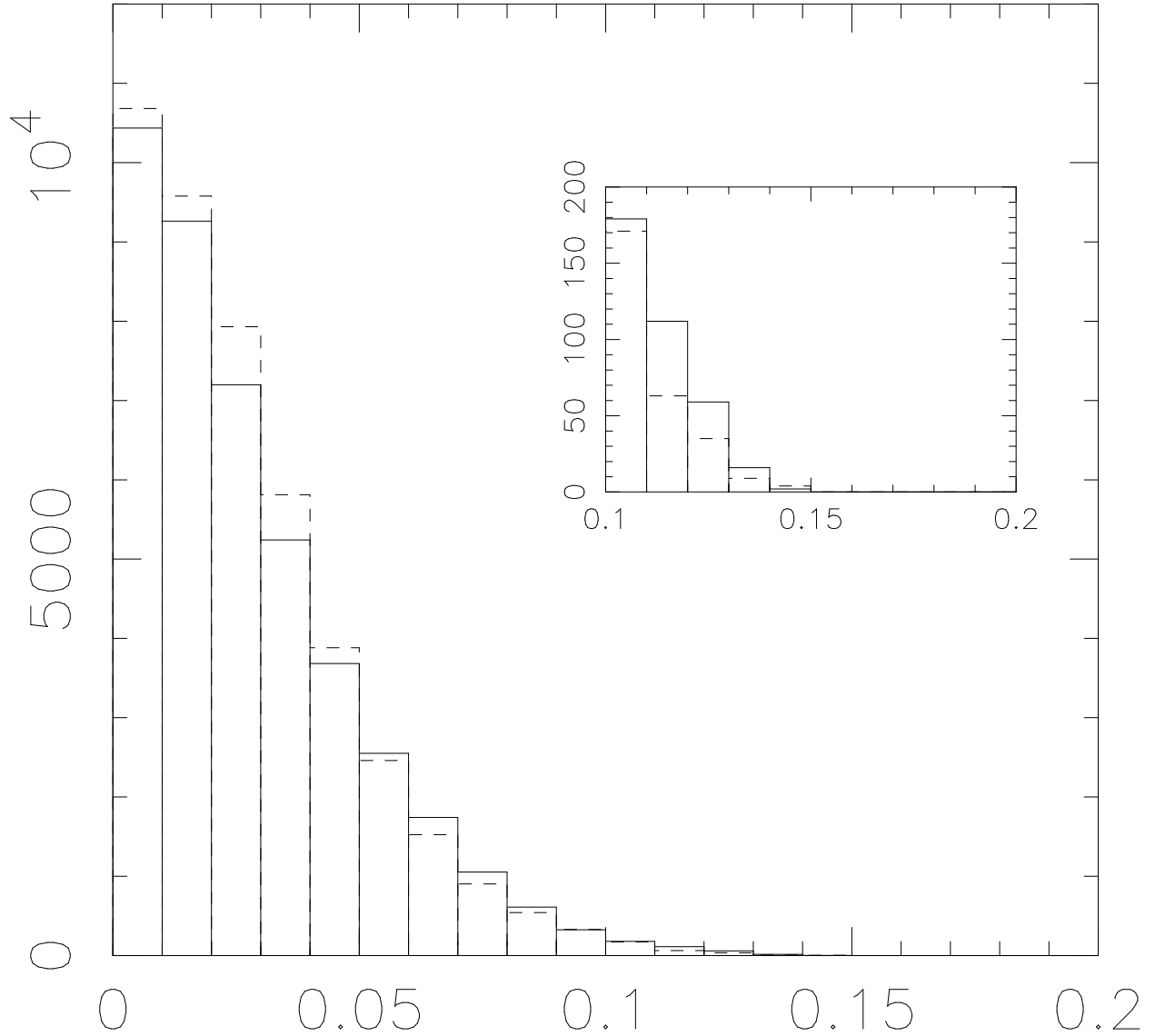


Fig. 8.— Histograms of absolute pixel values from the reconstructions of mass surface density  $\kappa$  using shear estimates from the  $IV$  catalogs (Figures 1 to 6). The solid histogram describes originally positive pixels and the dashed histogram describes originally negative pixels. The inset shows the contrast for extreme values. Clearly the distribution is very symmetrical. Notably, a highly positive tail is absent, indicating the absence of very overdense structures e.g. rich clusters.

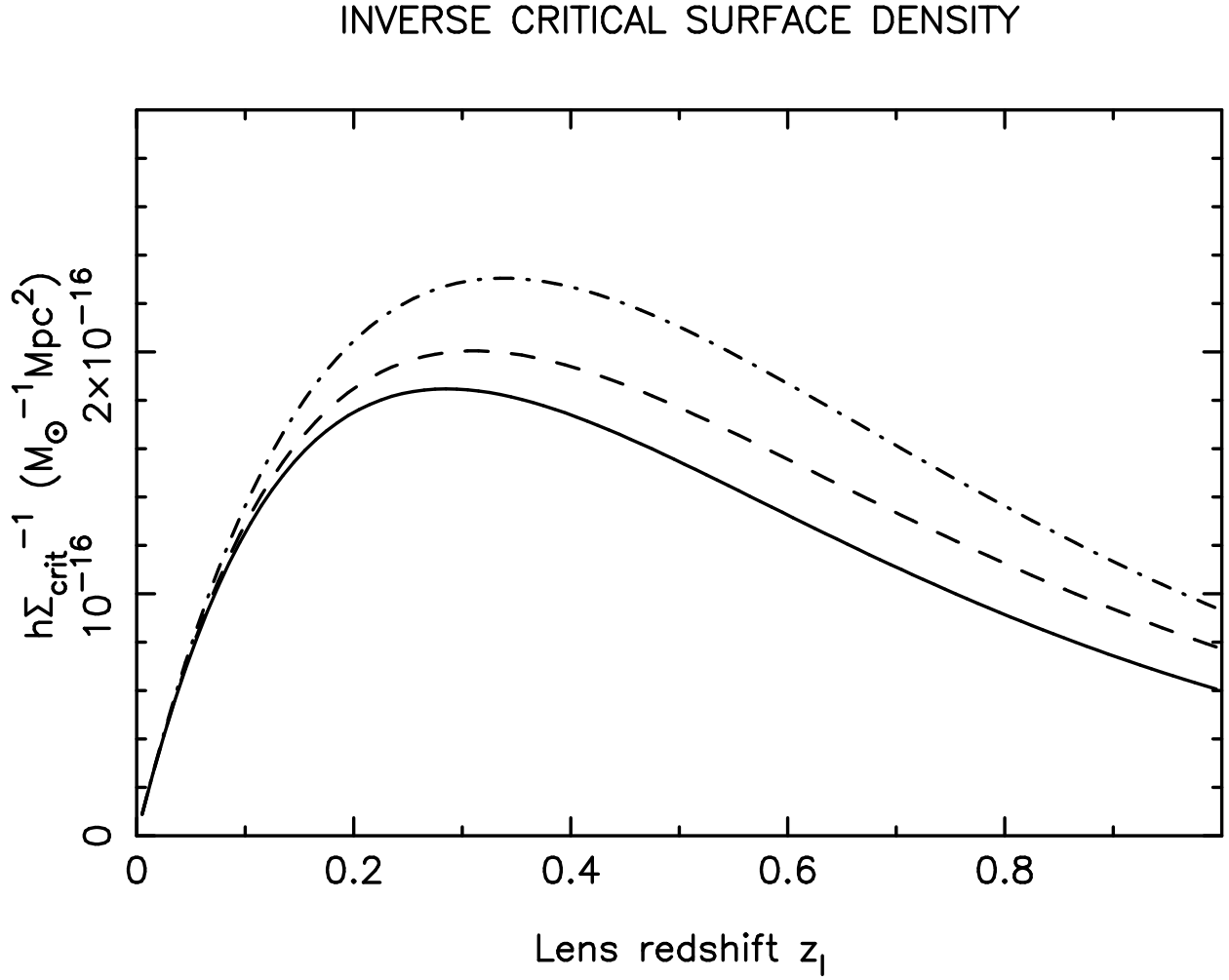


Fig. 9.— Inverse critical surface density,  $1/\Sigma_{\text{crit}}$ , as a function of redshift and cosmology using the analytic approximation to an  $m_I = 23$  source galaxy redshift distribution. Solid line is Einstein-deSitter ( $\Omega_{m0} = 1.0$ ,  $\Omega_{\lambda0} = 0.0$ ), dashed is open baryon ( $\Omega_{m0} = 0.05$ ,  $\Omega_{\lambda0} = 0.0$ ), dot-dashed is flat lambda ( $\Omega_{m0} = 0.3$ ,  $\Omega_{\lambda0} = 0.7$ ).

Fig. 10.— Upper left panel shows the predicted mass surface density using early type galaxies selected by  $V - I$  color, and  $M/L_B = 300 hM_\odot/L_\odot$  (see section 3.1 for details) for Lockman field (pointing 1). The image has been smoothed with a  $45''$  Gaussian filter. The mean has been subtracted from the image. The wedge shows the calibration of the grayscale and the contour separation is  $0.007 \times \Sigma/\Sigma_{\text{crit}}$ . The remaining three panels show the predicted surface mass density using early type galaxies and  $M/L_B = 300 hM_\odot/L_\odot$  but subdividing the galaxies into  $z = 0.2, 0.5, 0.8 \pm 0.15$ .

Fig. 11.— Same as for Figure 10 but for Lockman field (pointing 2).

Fig. 12.— Same as for Figure 10 but for Groth field (pointing 1).

Fig. 13.— Same as for Figure 10 but for Groth field (pointing 3).

Fig. 14.— Same as for Figure 10 but for 1650 field (pointing 1).

Fig. 15.— Same as for Figure 10 but for 1650 field (pointing 3).

Fig. 16.— Cross-correlation of light with mass reconstruction (left panel) and with randomized catalog reconstruction (right panel). The contour separation is  $1 \times 10^{-6}$  and the peak at zero lag is significant at the  $5.2\sigma$  level.

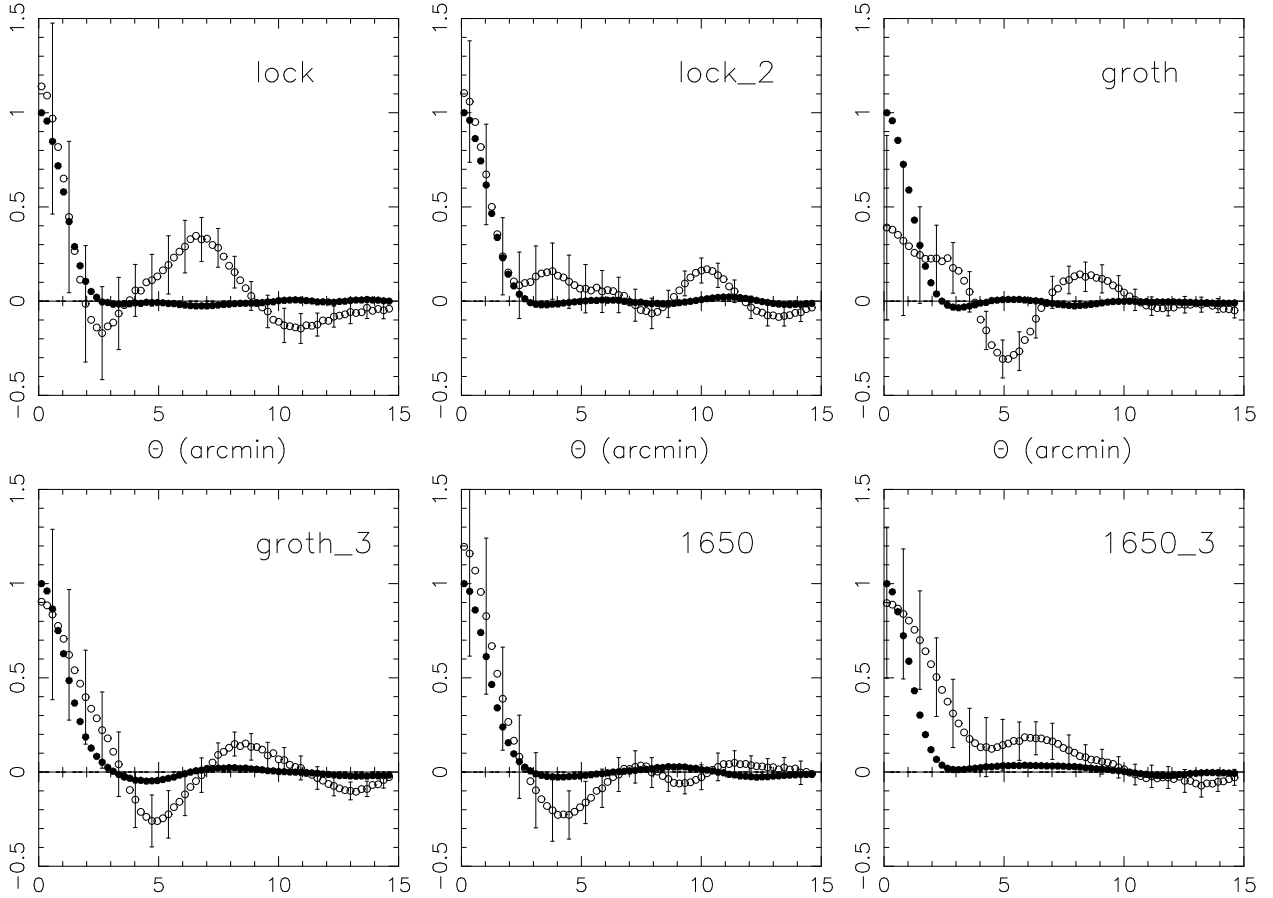


Fig. 17.— Azimuthally averaged profile of the mass-luminosity cross-correlation function (open circles with error bars) and the luminosity auto-correlation function (filled circles). In normalizing the mass-luminosity cross-correlation function we have adopted a  $M/L_B = 250 hM_\odot/L_\odot$ . For clarity, every third errorbar only is plotted.

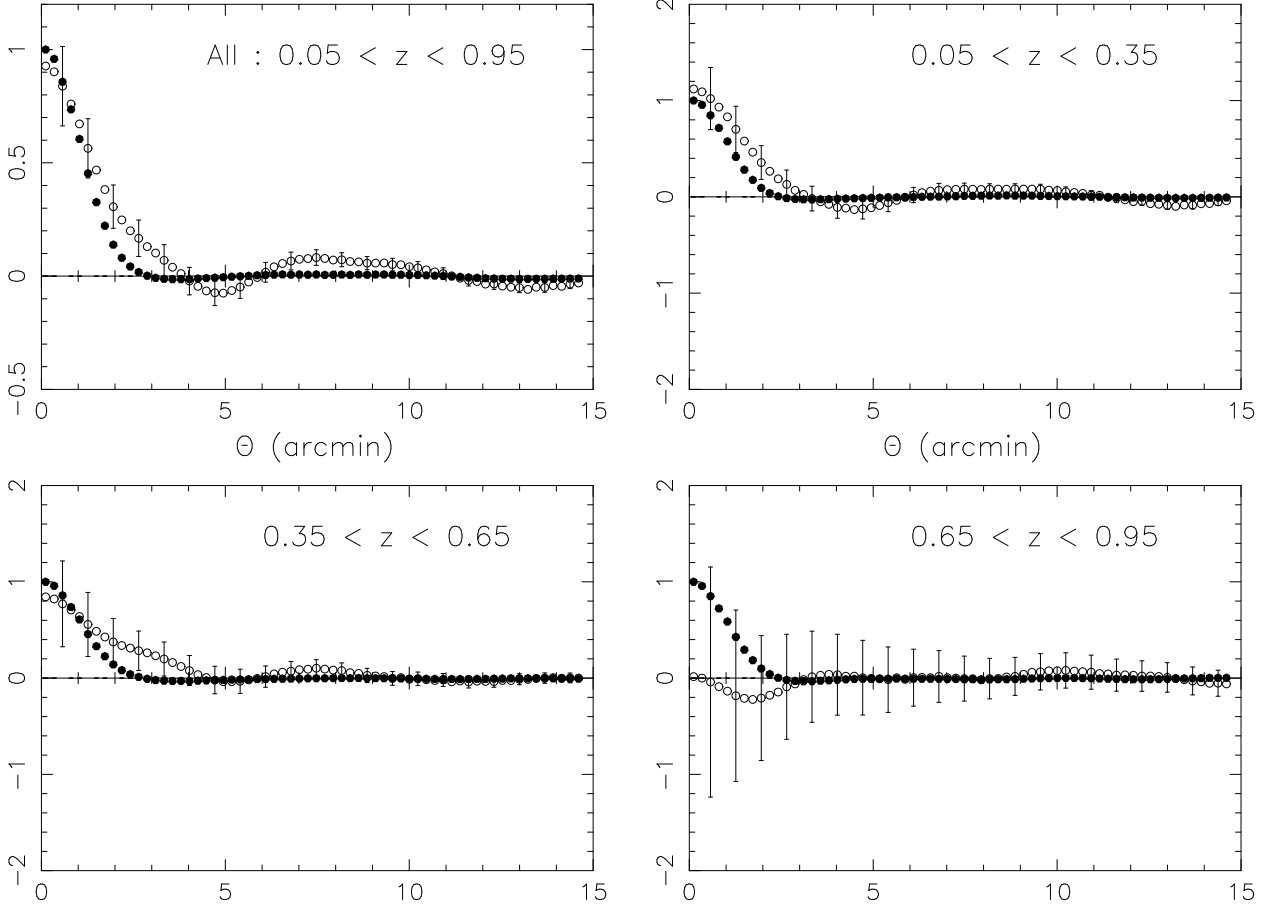


Fig. 18.— Azimuthally averaged profile of the mass-luminosity cross-correlation function from Figure 16 (open circles with error bars) and the luminosity auto-correlation function (filled circles). Upper left panel is for all galaxies (adopting a normalization  $M/L_B = 250 hM_\odot/L_\odot$ ), other panels are for redshift intervals as marked (adopting a normalization  $M/L_B = 300 hM_\odot/L_\odot$ ). Note change of abscissa scale. For clarity, every third errorbar only is plotted.

Fig. 19.— As for Figure 16 but cross-correlation of light from galaxies in redshift intervals  $z = 0.2, 0.5, 0.8 \pm 0.15$  with mass reconstruction (left panel) and with randomized catalog reconstruction (right panel). The contour separation is  $5 \times 10^{-7}$ . A correlation is seen between light and mass for galaxies at low and intermediate redshifts but no correlation is apparent for galaxies in the highest redshift interval.

This figure "fig1.gif" is available in "gif" format from:

<http://arxiv.org/ps/astro-ph/0102396v1>

This figure "fig2.gif" is available in "gif" format from:

<http://arxiv.org/ps/astro-ph/0102396v1>

This figure "fig3.gif" is available in "gif" format from:

<http://arxiv.org/ps/astro-ph/0102396v1>

This figure "fig4.gif" is available in "gif" format from:

<http://arxiv.org/ps/astro-ph/0102396v1>

This figure "fig5.gif" is available in "gif" format from:

<http://arxiv.org/ps/astro-ph/0102396v1>

This figure "fig6.gif" is available in "gif" format from:

<http://arxiv.org/ps/astro-ph/0102396v1>

This figure "fig7.gif" is available in "gif" format from:

<http://arxiv.org/ps/astro-ph/0102396v1>

This figure "fig10.gif" is available in "gif" format from:

<http://arxiv.org/ps/astro-ph/0102396v1>

This figure "fig11.gif" is available in "gif" format from:

<http://arxiv.org/ps/astro-ph/0102396v1>

This figure "fig12.gif" is available in "gif" format from:

<http://arxiv.org/ps/astro-ph/0102396v1>

This figure "fig13.gif" is available in "gif" format from:

<http://arxiv.org/ps/astro-ph/0102396v1>

This figure "fig14.gif" is available in "gif" format from:

<http://arxiv.org/ps/astro-ph/0102396v1>

This figure "fig15.gif" is available in "gif" format from:

<http://arxiv.org/ps/astro-ph/0102396v1>

This figure "fig16.gif" is available in "gif" format from:

<http://arxiv.org/ps/astro-ph/0102396v1>

This figure "fig19.gif" is available in "gif" format from:

<http://arxiv.org/ps/astro-ph/0102396v1>